



Ground-state power quenching in two-state lasing quantum dot lasers

Mariangela Gioannini

Citation: *J. Appl. Phys.* **111**, 043108 (2012); doi: 10.1063/1.3682574

View online: <http://dx.doi.org/10.1063/1.3682574>

View Table of Contents: <http://jap.aip.org/resource/1/JAPIAU/v111/i4>

Published by the [American Institute of Physics](#).

Related Articles

Detecting and tuning anisotropic mode splitting induced by birefringence in an InGaAs/GaAs/AlGaAs vertical-cavity surface-emitting laser

J. Appl. Phys. **111**, 043109 (2012)

85°C error-free operation at 38Gb/s of oxide-confined 980-nm vertical-cavity surface-emitting lasers

Appl. Phys. Lett. **100**, 081103 (2012)

Ultrafast response of tunnel injected quantum dot based semiconductor optical amplifiers in the 1300nm range

Appl. Phys. Lett. **100**, 071107 (2012)

Highly tunable whispering gallery mode semiconductor lasers with controlled absorber

Appl. Phys. Lett. **100**, 061112 (2012)

A capillary absorption spectrometer for stable carbon isotope ratio ($^{13}\text{C}/^{12}\text{C}$) analysis in very small samples

Rev. Sci. Instrum. **83**, 023101 (2012)

Additional information on *J. Appl. Phys.*

Journal Homepage: <http://jap.aip.org/>

Journal Information: http://jap.aip.org/about/about_the_journal

Top downloads: http://jap.aip.org/features/most_downloaded

Information for Authors: <http://jap.aip.org/authors>

ADVERTISEMENT

	Working @ low temperatures? Contact Janis for Cryogenic Research Equipment Click here to browse our site at www.janis.com	
---	---	---

Ground-state power quenching in two-state lasing quantum dot lasers

Mariangela Gioannini^{a)}

Dipartimento di Elettronica, Politecnico di Torino, Torino 10129, Italy

(Received 17 October 2011; accepted 7 December 2011; published online 22 February 2012)

The paper analyses theoretically the quenching of the ground state (GS) power observed in InAs/GaAs quantum dot lasers when emitting simultaneously from both ground state and excited state. The model, based on a set of rate equations for the electrons, holes, and photons, shows that the power quenching is caused by the different time scales of the electron and hole intra-level dynamic, as well as by the long transport time of the holes in the GaAs barrier. The results presented also evidence how the very different dynamics of electrons and holes have other important consequences on the laser behavior; we show for example that the electron and hole carrier densities of the states resonant with lasing modes are never clamped at the threshold value, and that the damping of relaxation oscillations is strongly influenced by the hole dynamics.

© 2012 American Institute of Physics. [doi:10.1063/1.3682574]

I. INTRODUCTION

Semiconductor lasers realized with self-assembled InAs quantum dots (QD) grown on a GaAs substrate have been intensively studied in the last ten years. One of the interesting properties of QD lasers, respect to the quantum well counterpart, is the possibility of achieving two-state lasing¹⁻³ or three-state lasing.⁴ It means that lasing starts at low current injection from the ground state (GS) transition; then, increasing current, the lasing can occur simultaneously also from the first excited state (ES₁) and sometimes from the second excited state (ES₂).⁴ This effect can be achieved in QD lasers because, as shown in Refs. 1 and 5, the carrier density in the states not resonant with the lasing modes (i.e., upper excited states, ground states of non-lasing dots) is not clamped at the value of the GS threshold, but it increases with current allowing other longitudinal modes, at the ES lasing transition, to reach the threshold condition. This two- or three-color lasing can be positively exploited in broad band comb lasers^{3,6-8} or in the realization of THz sources.⁹ Indeed in Refs. 3, 6, and 7, the wide emission spectrum of the comb laser is obtained thanks to the wide inhomogeneous broadening of the gain spectrum as well as through the simultaneous lasing from both GS and ES₁. In Ref. 9, the THz source is realized through the beating of the GS and the ES lasing modes of a multi-section QD-DFB laser. For these applications it is fundamental obtaining operation conditions where both GS and ES power equalize. Several experiments have, however, shown that whenever the ES reaches threshold the GS power starts reducing.^{1,2} To the best of our knowledge, this GS roll-off is not well understood yet. A simple exciton approximation used to model the laser could indeed only predict the saturation of the GS power after the ES threshold.¹⁰ For this reason, in Ref. 2, the measured GS roll-off could be reproduced by the exciton model only assuming a significant increase of the homogeneous broadening of the optical gain with increasing current. This depend-

ence of the homogenous broadening with the number of carriers in the active region was confirmed by theory and experiments.^{11,12} However, in the laser case, this dependence may be not as strong as was assumed in Ref. 2 and/or it is not the sole effect causing the GS power quenching.¹³ Viktorov *et al.*¹³ modeled the QD laser with separate rate equations for the electrons and for the holes, and they showed that the asymmetry in the rate of carrier redistribution among the energy levels of the electrons and holes leads to the formation of negatively charged excitons (*one electron-hole pair recombines leaving one additional electron*¹³). In Ref. 13, the excess electron was made to escape out of the GS via a *phenomenological linear decay rate of the carrier population*¹³ and it was “*necessary to reproduce the experimentally observed decrease of the GS emission.*”¹³ This decay rate was attributed to several possible effects (thermal re-emission in the wetting layer (WL), Auger depopulation, electron spin relaxation...) but, without modeling any of them, the authors could not verify if these effects are actually responsible for the GS power reduction. In Ref. 13, it was also assumed that the electrons and holes are directly injected in the ES₁; this assumption implies that only GS and ES₁ compete for the same carrier. This is not true for the holes, because the holes can thermalize quite fast among the several closely spaced states confined in the QD and in the wetting layer.^{14,15} With injection directly in ES₁, Ref. 13 also neglects the carrier transport across the barrier, whereas other works have shown that the transport time in the barrier is quite important to correctly model the dynamics of QD lasers.^{16,17}

In this paper, we present a rate-equation model that accounts for the important effects mentioned above and not included in Ref. 13 (in particular the thermalization of the holes and the carrier transport). Our goal is reproducing and explaining the measured GS-roll off when lasing occurs from both GS and ES. We will show that the roll-off is simply the consequence of the de-synchronization between the electron and hole dynamics, and that it is not necessary introducing any additional phenomenological decay of the carrier as done in Ref. 13. The de-synchronization between

^{a)}Author to whom correspondence should be addressed. Electronic mail: mariangela.gioannini@polito.it.

electrons and holes has been already evidenced in Ref. 18 but for a QD laser with emission only from GS, because the authors neglected all the excited states both in conduction and valence band.¹⁸ The assumption of just one confined state in the dots (the GS) is a heavy approximation for the InAs/GaAs QDs, in particular, in valence band where we have several closely spaced states confined in the QD.^{15,19} In this paper, we present several simulation results that will show how the de-synchronization between electron and hole dynamics, together with a long transport time in the GaAs barrier, has important consequences on the laser L-I characteristics as well as on the turn-on dynamics of the laser. The results shown will be also validated with a comparison with the experiments. The results presented in this work are not reproducible with the simple rate equation models²⁰ generally used to model bulk or quantum well lasers, and to the best of our knowledge they are peculiar of the QD material.

The paper is organized as follows: in Sec. II, we discuss the rate equation model used to analyze the QD laser, in Sec. III, we present the material and device parameter we used for the simulations; in Secs. IV and V, we show and discuss the numerical results focusing on the two-state lasing operation in both static (Sec. IV) and dynamic (Sec. V) operation conditions. Once we have understood which important parameters can control the GS roll-off, in Sec. VI, we will validate the model proposed with a comparison with the experiments. Finally in Sec. VII, we draw the conclusions.

II. NUMERICAL MODEL

We model the carrier and photon dynamics of the laser with a system of rate equations as generally done for QD lasers working at room temperature.^{15,16,21} A schematic of the conduction band and valence band diagram is shown in Fig. 1; on the same figure we also report the variable names representing the carrier density in the states (used in the rate equations that follows) together with the time constants for the capture and relaxation processes.

We have considered in conduction band two states confined in the QD (GS and ES), a wetting layer state and a bulk state due to the separate confinement hetero-structure (SCH). The energy separations between GS and ES as well as between ES and WL are set to 40 meV. The energy separation between the bottom of the WL band and the bottom of the SCH band is set to 200 meV. In valence band, we have the GS and four excited states ($ES_{1,...,4}$) confined in the QD; a WL state and a SCH state. The energy separation among valence band confined states and between the ES_4 and the WL state is set equal to 10 meV. The SCH state is separated by 140 meV respect to the WL. Even if the value of the energy separation among the states is quite dependent on the QD size and composition, the number used here are quite typical for InAs QD grown on GaAs.²²

The system of rate equations for the electrons in conduction band consists of two rate equations for the SCH and the WL, respectively, and four rate equations for the ES and GS. We have four rate equations because we divide the QD ensemble in two groups: the lasing QDs (i.e., the collection of

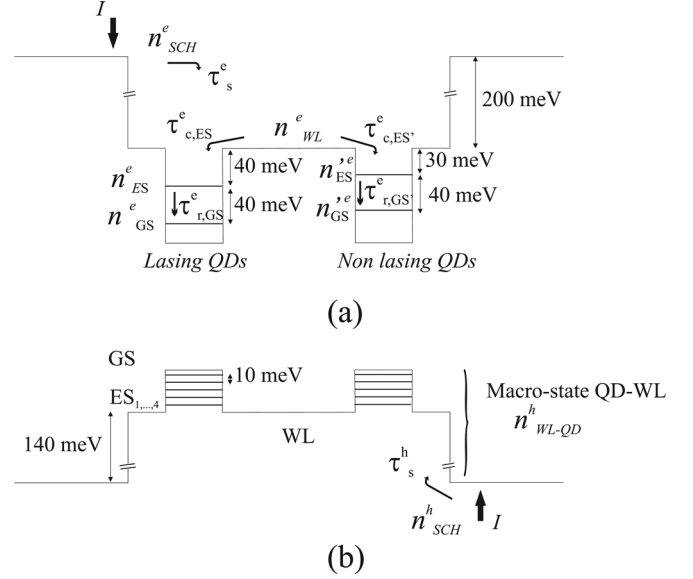


FIG. 1. Schematic of the (a) conduction band and (b) valence band diagram with the carrier densities and capture and relaxation time constants used in the rate equation system.

all the QD that reach the threshold condition) and the non-lasing QD (i.e., the collection of all the QD that can never reach threshold due to the low gain). We have used here a simplified approach respect to the more detailed multi-population rate equation model published in our previous works,^{15,23} because the purpose of this work is just focusing on how the GS and the ES of the same dot compete for the lasing and we want to neglect the competition for lasing between QD of different size.²⁴

To further simplify the model, we also assume that due to the fast thermalization of the holes among the several closely spaced states in valence band, we can collect the hole QD states and the WL state in one macro-state described with only one carrier rate equation.¹⁵ This approximation does not change the general conclusions and helps significantly in saving computation time. Therefore for the valence band, we have one rate equation for the holes in the SCH and one for the holes in the macro-state WL + QD. Based on this assumption, the system of rate equations for the carriers reads as follows:

$$\frac{dn_{SCH}^e}{dt} = \eta_i \frac{I}{n_d n_l w L} - \frac{n_{SCH}^e}{\tau_s^e} + \frac{n_{WL}^e}{\tau_{esc,WL}^e}, \quad (1)$$

$$\begin{aligned} \frac{dn_{WL}^e}{dt} = & \frac{n_{SCH}^e}{\tau_s^e} - \frac{n_{WL}^e}{\tau_{esc,WL}^e} - \frac{n_{WL}^e}{\tau_{nr,WL}^e} - \frac{n_{WL}^e}{\tau_{c,ES}^e} [G_n (1 - \rho_{ES}^e) \\ & + G'_n (1 - \rho_{ES'}^e)] + \frac{n_{ES}^e}{\tau_{esc,ES}^e} + \frac{n_{ES'}^e}{\tau_{esc,ES'}^e}, \end{aligned} \quad (2)$$

$$\begin{aligned} \frac{dn_{ES}^e}{dt} = & \frac{n_{WL}^e}{\tau_{c,ES}^e} G_n (1 - \rho_{ES}^e) - \frac{n_{ES}^e}{\tau_{esc,ES}^e} - \frac{n_{ES}^e}{\tau_{r,GS}^e} (1 - \rho_{GS}^e) \\ & + \frac{n_{GS}^e}{\tau_{esc,GS}^e} (1 - \rho_{ES}^e) - R_{stES} - R_{spES} - \frac{n_{ES}^e}{\tau_{nr,ES}^e}, \end{aligned} \quad (3)$$

$$\frac{dn_{ES}^e}{dt} = \frac{n_{WL}^e}{\tau_{e,ES}^e} G_n' (1 - \rho_{ES}^e) - \frac{n_{ES}^e}{\tau_{esc,ES}^e} - \frac{n_{ES}^e}{\tau_{r,GS}^e} (1 - \rho_{GS}^e) + \frac{n_{GS}^e}{\tau_{esc,GS}^e} (1 - \rho_{ES}^e) - R_{stES}' - R_{spES}' - \frac{n_{ES}^e}{\tau_{nr,ES}^e}, \quad (4)$$

$$\frac{dn_{GS}^e}{dt} = \frac{n_{ES}^e}{\tau_{r,GS}^e} (1 - \rho_{GS}^e) - \frac{n_{GS}^e}{\tau_{esc,GS}^e} (1 - \rho_{ES}^e) - R_{stGS} - R_{spGS} - \frac{n_{GS}^e}{\tau_{nr,GS}^e}, \quad (5)$$

$$\frac{dn_{GS}^h}{dt} = \frac{n_{ES}^h}{\tau_{r,GS}^h} (1 - \rho_{GS}^h) - \frac{n_{GS}^h}{\tau_{esc,GS}^h} (1 - \rho_{ES}^h) - R_{stGS}' - R_{spGS}' - \frac{n_{GS}^h}{\tau_{nr,GS}^h}, \quad (6)$$

$$\frac{dn_{SCH}^h}{dt} = \eta_i \frac{I}{n_d n_{lWL}} - \frac{n_{SCH}^h}{\tau_s^h} + \frac{n_{WL-QD}^h}{\tau_{esc,WL-QD}^h}, \quad (7)$$

$$\frac{dn_{WL-QD}^h}{dt} = \frac{n_{SCH}^h}{\tau_s^h} - \frac{n_{WL-QD}^h}{\tau_{esc,WL-QD}^h} - R_{sp tot} - R_{st tot} - R_{nr tot}. \quad (8)$$

In the system above, we indicate with $n_k^{e,h}$ the number of carriers (electrons, e , or holes, h), normalized respect to the total number of QDs, in the state k ($k = \text{GS, ES, SCH, WL, WL-QD}$); the prime apex in Eqs. (4) and (6) indicates the group of non-lasing QDs; the subscript $k = \text{WL-QD}$ indicates the macro-state collecting the holes in the QD confined states plus the WL state. The terms G_n and G_n' indicates the fraction of lasing and non-lasing dots, respectively, with $G_n' = I - G_n$. All the time constants ($\tau_{s,c,r,esc,nr;k}^{e,h}$) appearing in the equations above are defined in Table I; the escape times from one state to the state above are calculated to guarantee the thermal equilibrium in the absence of current injection and carrier loss rates (i.e., radiative and non-radiative recombination).^{10,25}

The occupation of each electron state is defined by $\rho_{GS,ES}^e = n_{GS,ES}^e / \mu_{GS,ES} G_n$ with $\mu_{GS} = 2$ the degeneracy of the GS and $\mu_{ES} = 4$ the degeneracy of the ES. The terms $R_{stGS,ES}$ are the GS and ES stimulated emission rates; the

term $R_{spGS,ES}$ are the spontaneous emission rates. These terms couple the electron rate equations (1)–(6) with the hole rate equations (7) and (8), and the photon rate equations reported in the following Eqs. (9) and (10). The terms $R_{st tot}$ and $R_{sp tot}$ account for the total stimulated emission and the total spontaneous emission rates that burn the holes available in the macro-state WL-QD. They are calculated as: $R_{st tot} = R_{stGS} + R_{stES} + R_{stGS}' + R_{stES}'$ and $R_{sp tot} = R_{spGS} + R_{spES} + R_{spGS}' + R_{spES}'$. Finally, the term $R_{nr tot} = \frac{n_{GS}^e}{\tau_{nr,GS}^e} + \frac{n_{GS}^h}{\tau_{nr,GS}^h} + \frac{n_{ES}^e}{\tau_{nr,ES}^e} + \frac{n_{ES}^h}{\tau_{nr,ES}^h} + \frac{n_{WL}^e}{\tau_{nr,WL}^e}$ accounts for the total non-radiative recombination rate.

The rate equations for the number of emitted photons (normalized respect to the total number of QDs) associated to the photons emitted from the GS (s_{GS}) and from the ES (s_{ES}) of the lasing QDs are as follows:

$$\frac{ds_{ES}}{dt} = \beta_{sp} R_{spES} + g_{ES} s_{ES} - \frac{s_{ES}}{\tau_p}, \quad (9)$$

$$\frac{ds_{GS}}{dt} = \beta_{sp} R_{spGS} + g_{GS} s_{GS} - \frac{s_{GS}}{\tau_p}. \quad (10)$$

The coefficients $g_{GS,ES}$ account for the gain at the GS and ES emission wavelengths of the lasing dots. These gain coefficients are given by the contribution of the lasing dots plus the contribution of the non lasing QDs via the homogeneous broadening,

$$g_{GS,ES} = \frac{G_n (\rho_{GS,ES}^e + \rho_{GS,ES}^h - 1)}{\tau_{g,GS,ES}} + \frac{G_n' (\rho_{GS,ES}^e + \rho_{GS,ES}^h - 1)}{\tau_{g,GS,ES}} \gamma_{\text{hom}},$$

where $\tau_{g,GS,ES}$ are time constants that include the optical confinement factors, the group velocity, and the dipole matrix elements; the coefficient γ_{hom} is a dimensionless number, in the range between 0 and 1. This coefficient accounts for the contribution of the non-lasing QDs to the gain, at the lasing wavelength, via the homogeneous broadening of emission line of the non-lasing dots. In Eqs. (9) and (10), β_{sp} is the

TABLE I. List of parameters defined in the model with corresponding values used in the simulations presented in the paper.

Parameter	Value used in the model
Dot density per layer n_d	$4 \cdot 10^{10} \text{ cm}^{-2}$
Laser length L	3 mm
Waveguide width	3 μm
Fraction of lasing (G_n) and non-lasing (G_n') QDs	$G_n = 0.65$, $G_n' = 0.35$
Electron/hole transport time in the SCH (Ref. 19) $\tau_s^{e,h}$	5 ps (electron), 20 ps (hole)
Escape time from WL to SCH $\tau_{esc,WL}^{e,h}$	100 ps (electron), 250 ps (hole)
Capture time from WL to ES for electrons $\tau_{c,ES}^e$	0.6 ps
Escape time from ES to WL for electrons $\tau_{esc,ES}^e$	0.96 ps
Relaxation time from ES to GS for electrons $\tau_{r,GS}^e$	1 ps
Escape time from GS to ES for electrons $\tau_{esc,GS}^e$	2.32 ps
Carrier lifetime due to non-radiative recombination $\tau_{nr,WL,GS,ES}^e$	900 ps (WL), 2 ns (GS,ES)
Carrier lifetime due to spontaneous emission $\tau_{sp,GS,ES}$	2 ns (GS,ES)
Gain time constant $\tau_{g,GS,ES}$	5 ps (GS), 2.8 ps (ES)

spontaneous emission factor. The spontaneous emission rates are calculated as

$$R_{sp\,GS,ES} = \frac{G_n}{\tau_{sp\,GS,ES}} \mu_{GS,ES} \rho_{GS,ES}^e \rho_{GS,ES}^h,$$

$$R'_{sp\,GS,ES} = \frac{G'_n}{\tau_{sp\,GS,ES}} \mu_{GS,ES} \rho_{GS,ES}^{le} \rho_{GS,ES}^{lh}.$$

With these notations the stimulated emission terms in Eqs. (3)–(6) are written as

$$R_{st\,GS,ES} = G_n \frac{(\rho_{GS,ES}^e + \rho_{GS,ES}^h - 1)}{\tau_{g\,GS,ES}} s_{GS,ES},$$

$$R'_{st\,GS',ES'} = G'_n \frac{(\rho_{GS,ES}^{le} + \rho_{GS,ES}^{lh} - 1)}{\tau_{g\,GS,ES}} s_{GS,ES} \rangle_{hom}.$$

The parameter τ_p in Eqs. (9) and (10) is the photon lifetime²⁰ and accounts for the mirror loss as well as intrinsic loss of the waveguide.

Finally, the hole occupation of each state (ρ_k^h) is obtained assuming that the holes always thermalize, with quasi-Fermi level E_f^h , in the macro-state WL-QD;^{14,15} that is

$$\rho_k^h = \frac{1}{1 + e^{(E_k^h - E_f^h)/KT}}, \quad (11)$$

$$n_{WL-QD}^h = \delta_{WL}^h \log\left(1 + e^{(E_f^h - E_{WL}^h)/KT}\right) + \sum_{k=GS,ES,1,\dots,4} \mu_k^h \rho_k^h. \quad (12)$$

In Eqs. (11) and (12), we define E_k^h the energy level of the valence band k -state confined in the QD and with E_{WL}^h the energy of the valence band WL state; δ_{WL}^h is the two dimensional density of states of the holes in the WL normalized respect to the total number of QDs; KT is the thermal energy. At each time instant t we get n_{WL-QD}^h from Eq. (8), and then the quasi-Fermi level E_f^h from the numerical solution of Eq. (12).

III. SIMULATION PARAMETERS

In this section, we present the laser structure and the input parameters required by the model. In Table I, we list the material and device parameters with the definition of the parameters used in the rate equations (1)–(12).

Making reference to the values of the time constants reported in Table I for the electron/hole transport, capture, and relaxation, we evidence the strong difference between the electron time constants (all in the range of few picoseconds) and the hole time constants. The hole dynamics is indeed characterized by a quite slow diffusion in the GaAs barrier (leading to transport time of several pico-seconds) and an ultra-fast thermalization in the QD states. These different time scales of the electrons and holes cause a strong de-synchronization of the two populations after current and/or photon time variations.

In Sec. IV, we will show that the hole transport time (τ_s^h) is a key parameter for explaining the GS roll-off. For this reason, in Fig. 2, we report the modal gain at the GS and ES wavelength versus current injection calculated using τ_s^h as parameter. The modal gain has been calculated for three dif-

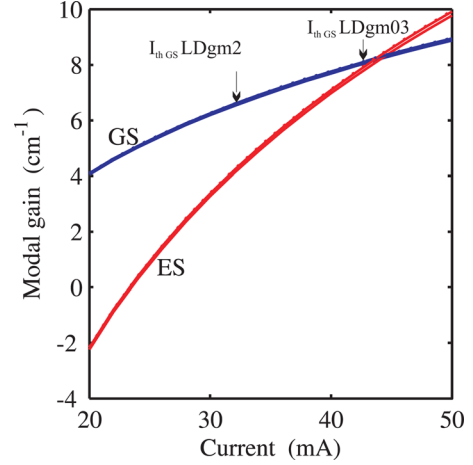


FIG. 2. (Color online) GS and ES net modal gain calculated for several values of τ_s^h (20 ps, 5 ps, and 0.5 ps); it is not possible to distinguish the curves for the different τ_s^h , because, without stimulated emission, the curves practically overlap. The arrows indicate the threshold condition for the lasers LD_{gm2} and LD_{gm03}.

ferent values of τ_s^h (20 ps, 5 ps, and 0.5 ps) but the traces obtained all practically overlap because, without lasing, at room temperature, the transport time (and more generally also the capture and relaxation time constants) poorly changes the gain property of the material. From this figure, we choose to simulate two different lasers: the first laser (LD_{gm03}) has photon life-time of Eqs. (9) and (10) $\tau_p = 14.55$ ps to guarantee a gain margin at the GS threshold of about 0.3 cm^{-1} ; the second laser (LD_{gm2}) has $\tau_p = 18.86$ ps which gives a gain margin of 2 cm^{-1} . The gain margin is defined as the difference between the GS and ES gain at the GS threshold current. As direct consequence of Fig. 2, we also observe that the gain margin is not changed by the transport time.

IV. SIMULATION OF THE STATIC CHARACTERISTICS OF TWO-STATE LASING

We plot in Figs. 3(a) and 3(b), the L-I characteristics for the laser LD_{gm03} and LD_{gm2} obtained for different values of the hole transport time τ_s^h . The Figures show that for high transport time (i.e., 20 ps) the GS power rolls off when the ES starts lasing; when the transport time reduces the slope of the rolling off reduces. With $\tau_s^h = 10$ ps, the power of the GS nearly saturates; whereas for smaller values (i.e., 5 ps or 0.5 ps) the GS power slightly increases after the ES threshold. On the same graph we also plot in black lines the total output power (sum of GS and ES power) in the three cases. The total output power is practically independent on τ_s^h because both GS and ES share the same carriers accumulated in the WL state which acts as the reservoir; the parameter τ_s^h only changes the amount of carriers available for the GS or the ES emission. Fig. 3 also confirms that the GS roll-off is not dependent on the gain margin and therefore on the photon lifetime (i.e., device length). Indeed, even if the two lasers have very different gain margins, the GS roll-off is controlled only by the hole transport time; increasing the gain margin the ES threshold moves to higher currents (Fig. 3(b)) but the GS roll-off remains for the case $\tau_s^h = 20$

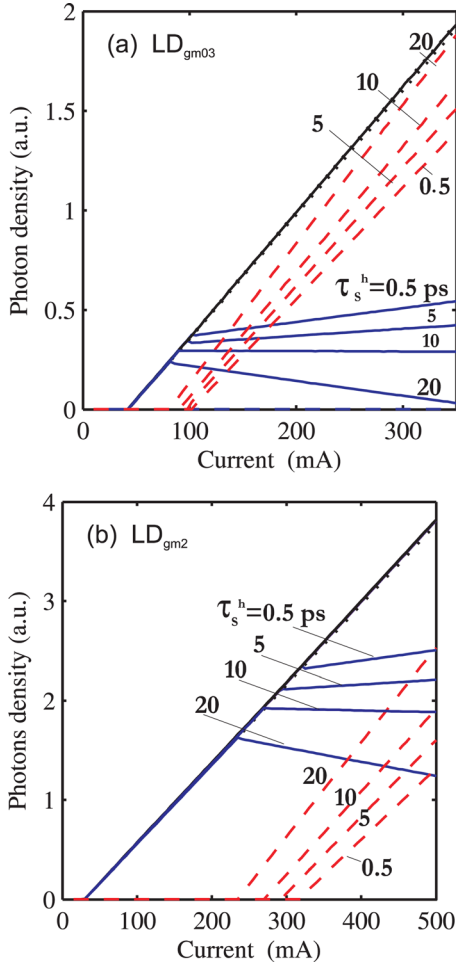


FIG. 3. (Color online) L-I characteristics of (a) LD_{gm03} and (b) LD_{gm2} calculated for different values of hole transport time τ_s^h ; blue line is the GS power; dashed red line is the ES power, and black dotted line is the total power (sum of GS and ES power). The curves of total power practically overlap for all values of τ_s^h .

ps. To the best of our knowledge, the role of the transport time, as a possible cause for the GS roll-off, has never been considered before in the literature. We believe that a value of $\tau_s^h = 20$ ps is quite reasonable for typical QD laser structures as those measured in Ref. 13. Assuming a barrier thickness (from p-doped to n-doped cladding) in the range between 400 nm and 500 nm and the electron and hole diffusion constants of 200 cm²/s and 10 cm²/s, respectively, we get with the model in Ref. 21, τ_s^e in the range between 1 ps and 1.5 ps and τ_s^h in the range between 20 ps and 30 ps. Measurements in Ref. 26 led an estimation of τ_s^h of about 15 ps for a barrier thickness of 100 nm.

We plot in Fig. 4(a) the GS and ES electron and hole occupation ($\rho_{GS,ES}^{e,h}$) as function of current for LD_{gm2} with $\tau_s^h = 20$ ps; in Fig. 4(b), we plot the GS and ES net modal gain as function of current. The figures evidence the following:

- (1) In the current range between I_{thGS} and I_{thES} only the GS is above threshold; therefore the GS gain is clamped (Fig. 4(b)), but, as shown in Fig. 4(a), the GS electron occupation, ρ_{GS}^e , decreases and the GS hole occupation ρ_{GS}^h increases up to the ES threshold (I_{thES}). The

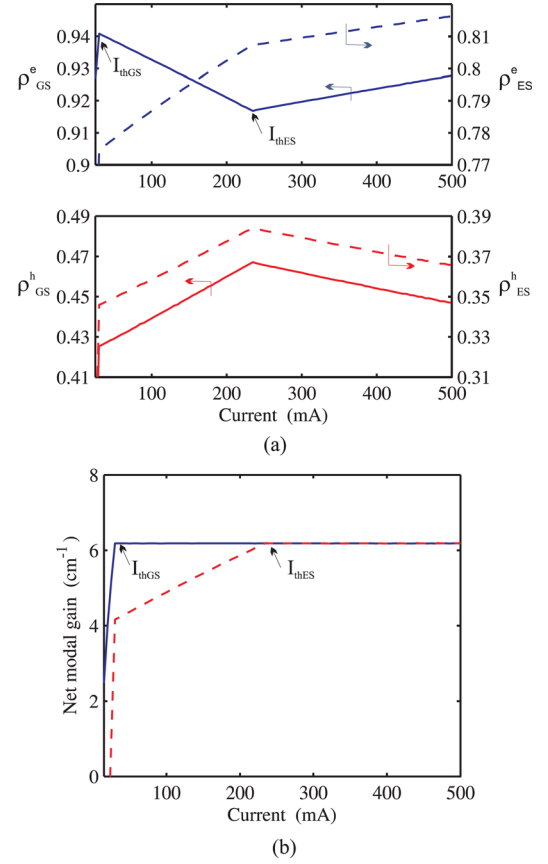


FIG. 4. (Color online) (a) Occupation probability of the electrons and holes in the GS and ES for laser LD_{gm2} and $\tau_s^h = 20$ ps and (b) corresponding GS (blue continuous line) and ES (red dashed line) net modal gain.

increase/decrease of GS electrons/holes compensates each other keeping the GS gain constant. This result is not obtainable with an exciton model and it is the consequence of the different time scale for the electron and the hole dynamics.¹⁸ In the current range between I_{thGS} and I_{thES} , the ES electrons and holes continue to increase (dashed lines of Fig. 4(a)) leading to the increase of the ES gain (Fig. 4(b)). The increasing electron density in the ES acts either as the source of electrons that feed the GS stimulated emission or as the carriers that, remaining in the ES, contribute to the increase of the ES gain.

- (2) Above I_{thES} , ρ_{GS}^e and ρ_{ES}^e both increase, while ρ_{GS}^h and ρ_{ES}^h both decrease. This happens because, when the ES starts lasing, the rate N_{SCH}^h/τ_s^h , which provides the holes in the WL-QD state, is not fast enough to compensate for the stimulated emission. As consequence of the reduction of the hole density, $\rho_{GS,ES}^e$ must increase to maintain the GS and the ES gain clamped at the threshold value.

The increase/decrease of $\rho_{GS,ES}^e/\rho_{GS,ES}^h$ above I_{thES} is controlled by the parameter τ_s^h and eventually causes the GS roll-off. As shown in Fig. 5, when we neglect the hole transport (i.e., setting $\tau_s^h = 0.5$ ps) the total hole density $\rho_{GS,ES}^h$ continue to increase even above I_{thES} . In this case, the increasing holes allow ρ_{GS}^e reducing and avoid the GS power quenching.

To better understand this behavior, we analyze which terms control the rate of GS emitted photons per unit of time.

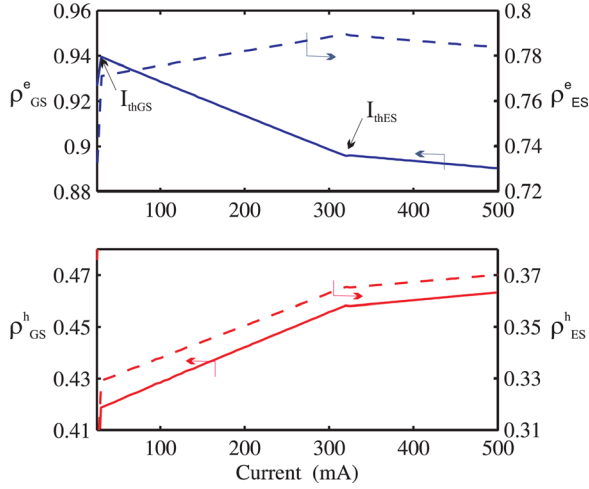


FIG. 5. (Color online) Occupation probability of the electrons and holes in the GS and ES for laser LD_{gm2} and $\tau_s^h = 0.5$ ps; in this case ρ_{GS}^e continue to reduce after I_{thES} .

Focusing on Eq. (5) in steady state and far above threshold, we can neglect the spontaneous emission and the non-radiative recombination; therefore the stimulated emission rate from the GS (R_{stGS}) equals the balance between the relaxation of carriers from ES and the carrier escape to the ES. Since the escape time constant is higher than the relaxation time constant, we can neglect the escape respect to the capture (this assumption has been verified in the simulated results). As a consequence, R_{stGS} is mainly fed by the rate of electron relaxation from the ES to the GS,

$$R_{stGS} \cong \frac{n_{ES}^e}{\tau_{r,GS}^e} (1 - \rho_{GS}^e). \quad (13)$$

The derivative $\partial R_{stGS} / \partial I$ gives how the GS stimulated emission changes with current; derivating Eq. (13) respect to the current we get

$$\frac{\partial R_{stGS}}{\partial I} = \frac{4G_n}{\tau_{r,GS}^e} \left[\frac{\partial \rho_{ES}^e}{\partial I} (1 - \rho_{GS}^e) - \rho_{ES}^e \frac{\partial \rho_{GS}^e}{\partial I} \right]. \quad (14)$$

From Fig. 4(a), above I_{thES} , we see that $\partial \rho_{ES}^e / \partial I$ is approximately equal to $\partial \rho_{GS}^e / \partial I$ and both derivatives are positive. However in Eq. (14), $\partial \rho_{ES}^e / \partial I$ is multiplied by $(1 - \rho_{GS}^e)$ with $\rho_{GS}^e \cong 0.91$ and $(1 - \rho_{GS}^e) = 0.09$, whereas $\partial \rho_{GS}^e / \partial I$ is multiplied by $\rho_{ES}^e \cong 0.79$. As a consequence, the term $\frac{4G_n}{\tau_{r,GS}^e} \left[\frac{\partial \rho_{ES}^e}{\partial I} (1 - \rho_{GS}^e) \right]$ is negligible compared to $\frac{4G_n}{\tau_{r,GS}^e} \left[-\rho_{ES}^e \frac{\partial \rho_{GS}^e}{\partial I} \right]$ and we get $\partial R_{stGS} / \partial I < 0$ (GS power decreasing with current). On the contrary, when $\tau_s^h = 0.5$ ps, we have, above I_{thES} , $\partial \rho_{GS}^e / \partial I < 0$ and $\partial R_{stGS} / \partial I > 0$ (GS power increasing with current). The case of Fig. 4 physically means that the increase of ρ_{GS}^e , necessary to compensate for the burning of holes, causes a reduction of the relaxation rate from the ES due to the increase of the Pauli blocking term $(1 - \rho_{GS}^e)$. The decreased relaxation rate reduces then the stimulated emission given by Eq. (13).

It is important to observe that the exciton models predict that ρ_{GS}^e is clamped above threshold^{2,10} (as it is very well

known from bulk and quantum well laser theory²⁰). Therefore, using an exciton model, the only possibility above I_{thES} is the saturation of the GS power ($\partial R_{stGS} / \partial I = 0$) because we have $\partial \rho_{ES}^e / \partial I = 0$ (ES carriers clamped above I_{thES}) and $\partial \rho_{GS}^e / \partial I = 0$ (GS carriers clamped above I_{thGS}). Here, we have shown that neither the electron density nor the hole density of the states involved in lasing are clamped but these densities increase or decrease such that the gain, dependent on the sum of electron and hole densities, remains clamped.

V. SIMULATION OF DYNAMIC CHARACTERISTICS OF TWO STATE LASING

To better understand the dynamics of the two-state lasing and to analyze further the effects of the electron and hole de-synchronization, we study the photon and carrier dynamics during the laser switch-on. In particular, we study here two types of transients; in the first transient, we consider the laser LD_{gm03} turned on with an injected current from 0 mA to $I_{thES} = 81$ mA. In the second transient, after biasing the laser at I_{thES} , we switch the current at a value much higher than I_{thES} , for example $3I_{thES}$. We focus on the case with $\tau_s^h = 20$ ps, that produces the GS roll-off. We plot in Fig. 6(a) the GS and ES power, when at time instant $t = 0$ ps, we inject a current step from zero to I_{thES} . As already evidenced

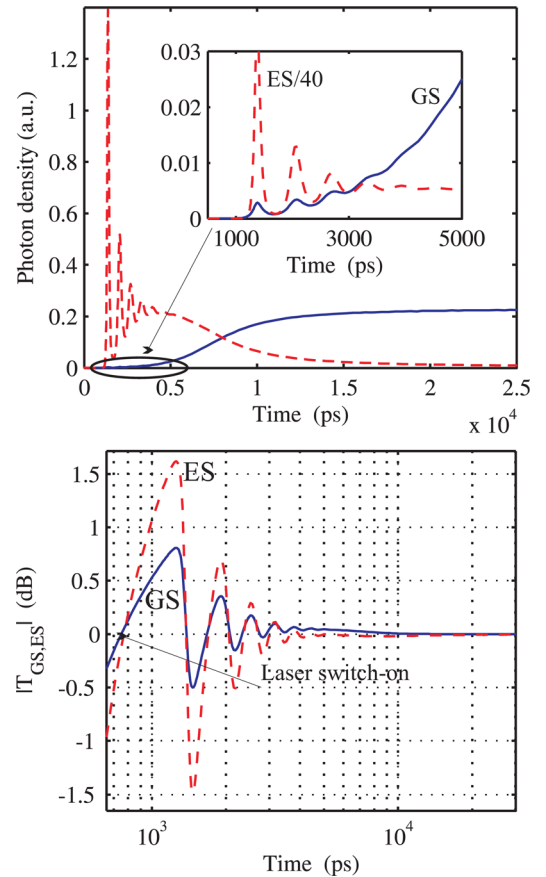


FIG. 6. (Color online) (a) GS (blue solid line) and ES (red dashed line) power after the laser is switched on, at $t = 0$ ps, with a current step from $I = 0$ to $I = I_{thES}$. (b) GS (blue solid line) and ES (red dashed line) round trip gain during the transient. The arrow in (b) indicates the time instant when round trip gain reaches unit for the first time. The laser considered is LD_{gm03} with $\tau_s^h = 20$ ps.

in Ref. 27, we have first a significant power emission from the ES; after a quite long transient of about 5 ns, the GS turns on with a consequent reduction of the ES power. When the GS power reaches steady state the ES power is approximately zero. We plot in Fig. 6(b) the GS and ES round trip gain ($T_{GS,ES}$) of the laser defined from Eqs. (9) and (10) as

$$T_{GS,ES} = g_{GS,ES} \times \tau_p. \quad (15)$$

Figure 6(b) shows that both GS and ES reach the threshold condition of round trip gain equal to unit ($|T_{GS,ES}| = 1$) at almost the same time (time instant indicated with the arrow in Fig. 6(b)) and therefore the two states switch on practically together (see the inset of Fig. 6(a)). However, after the switch on, the ES round trip gain grows faster respect to the GS round trip gain, because the ES has higher differential gain and because the ES collects electrons before the GS. This causes the fast increase of the ES power. On the contrary, the growth of $|T_{GS}|$ above unit is slower as seen in Fig. 6(b). Therefore, the GS starts lasing simultaneously with the ES but with an extremely low power (see inset of Fig. 6(a)); this power is also increasing very slowly with time compared to the ES. At time instant $t \cong 5$ ns, the stimulated emission from the GS gets however strong enough such that the carrier relaxation from the ES starts dominating respect to the stimulated emission from the ES. Therefore, the carrier density in the ES reduces causing the complete ES switch-off with $|T_{ES}|$ slightly below 1. If now, in this new steady state condition, we inject further current, the additional carriers can restore the lasing condition also for the ES, which will lase simultaneously with the GS. This is shown in Fig. 7, where we plot the transient after switching the current, at $t = 40$ ns, from I_{thES} to $3I_{thES}$. We observe that the total output power reaches steady state after about 1.5 ns, whereas the transient of the GS and ES power are longer (about 4 ns). The dynamics of the total stimulated emission rate depends indeed on the total number of carriers injected in the QD and it is almost driven by the hole dynamics because, as shown in the inset of Fig. 7, the variation of the GS + ES hole den-

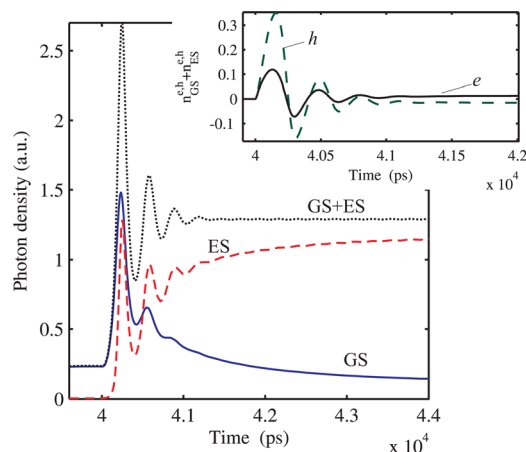


FIG. 7. (Color online) GS (blue solid line), ES (red dashed line), and total (black dotted line) output power during the transient after a current step at $t = 40$ ns from I_{thES} to $3I_{thES}$. The laser considered is the same of Fig. 5. The inset shows variation (after the current step) of the number of holes (dashed line) and electrons (solid line) in the states GS + ES.

sity is higher compared to the GS + ES electron density. Furthermore, when the total carriers in GS + ES reach the steady state, the total power reaches steady state as well. On the contrary, as we will discuss later, the dynamics of GS and ES power (blue solid and red dashed lines in Fig. 7) is dominated by the way the carriers in the QD redistribute between the GS and the ES.

To highlight the role of the electron and hole desynchronization and the role of the hole transport time in the power dynamics, we plot in Figs. 8(a) and 8(b) the phase portraits,¹⁸ in the plane $(\Delta\rho_{GS}^{e,h}, \Delta s_{GS})$, of the switching dynamic of the GS power when the current switches with a step from I_{thES} to $I_{thES} + 170$ mA. We consider the cases with $\tau_s^h = 20$ ps in Fig. 8(a), and the case with $\tau_s^h = 0.5$ ps in Fig. 8(b). In both cases, starting from the steady state at I_{thES} , we give the same current of 170 mA, to be sure that the

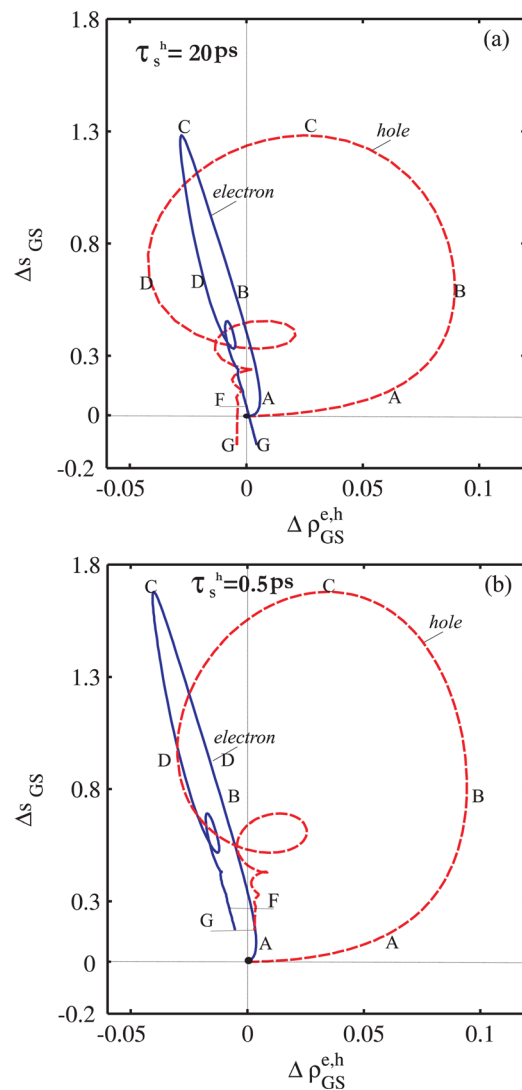


FIG. 8. (Color online) Phase portrait of the switching dynamics after current step from I_{thES} to $I_{thES} + 170$ mA in the plane $(\Delta\rho_{GS}^{e,h}, \Delta s_{GS})$ for the laser LD_{gm03} with (a) $\tau_s^h = 20$ ps and (b) $\tau_s^h = 0.5$ ps. In each figure, the pair of points marked with the same letter indicates the same time instant in the electron (blue solid line) and hole (red dashed line) traces. The bold circle in (0, 0) indicates the point where the transient starts (i.e., steady state point at I_{thES}).

number of carriers, added per unit of time respect to the ES threshold, is the same.

In Figs. 8(a) and 8(b), we define $\Delta\rho_{GS}^{e,h}$ as the deviation of $\rho_{GS}^{e,h}$ respect to the value at the I_{thES} , it means

$$\Delta\rho_{GS}^e = \rho_{GS}^e - \rho_{GS}^e|_{thES} \text{ and } \Delta\rho_{GS}^h = \rho_{GS}^h - \rho_{GS}^h|_{thES}.$$

In the same way Δs_{GS} is defined as the deviation of the photon density respect to the steady state value at I_{thES}

$$\Delta s_{GS} = s_{GS} - s_{GS}|_{thES}.$$

The point $(\Delta\rho_{GS}^{e,h} = 0, \Delta s_{GS} = 0)$ corresponds to the steady state at I_{thES} ; any pair of points (one point in the electron phase portrait and one point in the hole phase portrait), with the same Δs_{GS} and $\Delta\rho_{GS}^e + \Delta\rho_{GS}^h = 0$ corresponds to the condition $|T_{GS}| = 1$, and therefore to a maximum (for example points with letter C in Fig. 8) or a minimum of s_{GS} or to the new steady state solution (points indicated with letter G in Fig. 8). The pairs of points with the same Δs_{GS} and $\Delta\rho_{GS}^e + \Delta\rho_{GS}^h > 0$ corresponds to $|T_{GS}| > 1$ (i.e., power increasing with time); *vice versa* the pairs with same Δs_{GS} and $\Delta\rho_{GS}^e + \Delta\rho_{GS}^h < 0$ corresponds to $|T_{GS}| < 1$ (i.e., power decreasing with time).

The phase portraits in Fig. 8 can be read as follows:

- (1) Starting from the steady state at I_{thES} (bold circle in $\Delta\rho_{GS}^{e,h} = 0, \Delta s_{GS} = 0$) the power increases as the consequence of the current step. However, the GS electrons respond with a just very small increase (up to point A), while the hole density continues to increase significantly up to point B. The limited increase of the electron occupation is almost caused by the blocking term $(1 - \rho_{GS}^e)$, which is close to zero. For the electrons, the path from A to C is dominated by the burning of carriers due to stimulated emission; whereas the burning of holes starts later in point B.
- (2) After point C the GS electrons begin to recover thanks to the electrons available in the ES (path from C to G). On the contrary, the GS holes continue to be burned by the total stimulated emission rate up to point D. The recovery of electrons (path from C to G) is almost linear with power implying that the electron dynamics causes a strong damping of the power relaxation oscillations; on the contrary the recovery of the holes follows a more complex dynamics (“curly” path from D to F) implying that the holes contribute to enhance the amplitude of the relaxation oscillations of the GS power (reduction of the damping factor). Comparing the hole path from B to D in the case $\tau_s^h = 20$ ps and $\tau_s^h = 0.5$ ps in Fig. 9, we see that the burning of holes (from B to D) is stronger with $\tau_s^h = 20$ ps, because in this case the variation of the hole density from B to D is bigger respect to the case with $\tau_s^h = 0.5$ ps. This is because with $\tau_s^h = 20$ ps, the slower hole transport time can not balance the fast loss of holes due to stimulated emission.
- (3) In point F of Fig. 8, the hole density reaches the new steady state value because from F to G the path is a vertical line with no variation of GS holes nevertheless a continue decrease of the GS power. This is because in point

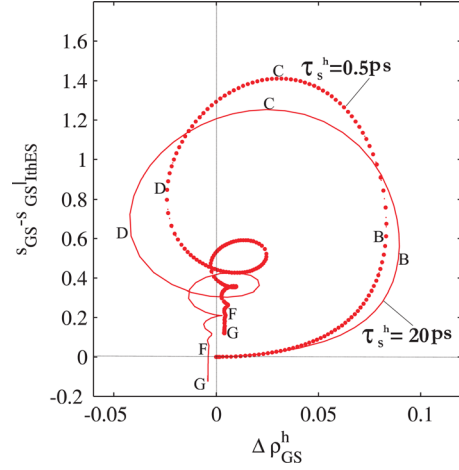


FIG. 9. (Color online) Comparison of the phase portraits of the switching dynamics after current step from I_{thES} to $I_{thES} + 170$ mA in the plane $(\Delta\rho_{GS}^h, s_{GS})$ to evidence the differences in the GS hole dynamics between the case $\tau_s^h = 20$ ps (thin solid line) and $\tau_s^h = 0.5$ ps (thick dotted line). The letters are the same of Fig. 7(a) (thin solid line) and Fig. 7(b) (thick dotted line).

F the total emitted power, governing the burning of the holes in the QD-WL state, reaches the new steady state condition while the GS power continue to decrease because we have $\Delta\rho_{GS}^e + \Delta\rho_{GS}^h|_F < 0$. Therefore, the electrons need to grow further (path from F to G) to guarantee the steady state lasing condition with $\Delta\rho_{GS}^e + \Delta\rho_{GS}^h|_G = 0$. The electron and hole density in the points F of Figs. 8(a) and 8(b) are however different. In Fig. 8(a), we have $\Delta\rho_{GS}^h|_F < 0$ and $\Delta\rho_{GS}^e|_F \cong 0$; whereas in Fig. 8(b), we have $\Delta\rho_{GS}^h|_F > 0$ and $\Delta\rho_{GS}^e|_F < 0$. Therefore, in Fig. 8(a), the GS electrons need to grow more respect to Fig. 8(b) to guarantee $\Delta\rho_{GS}^e + \Delta\rho_{GS}^h = 0$; this further growth causes the GS power to decrease more in the path from F to G in Fig. 8(a) respect to the same path in Fig. 8(b). For this reason, in point G (steady state solution $I_{thES} + 170$ mA) of Fig. 8(a) the power is necessarily lower than in the starting point represented by the bold circle. This can explain the GS roll-off in the L-I of Fig. 3(a).

The phase portraits reported in Fig. 8 are quite general, because we have seen that this qualitative behavior is maintained also changing the gain margin and/or the time constant governing the electron and hole dynamics as soon as we assume that the holes dynamics inside the QD is much faster than the electron dynamics. More generally, we believe that these pictures may be also useful to understand how the electrons and the hole contribute very differently to the dynamics of the laser. This definitely shows that the exciton model is a too simplified approximation for modeling correctly a QD laser dynamic.

VI. COMPARISON WITH THE EXPERIMENTS

The simulation results shown in Secs. IV and V have been useful to understand the mechanisms behind the two-state lasing effect in QD lasers. To validate our model we finally compare in Fig. 10 the measured and simulated L-I

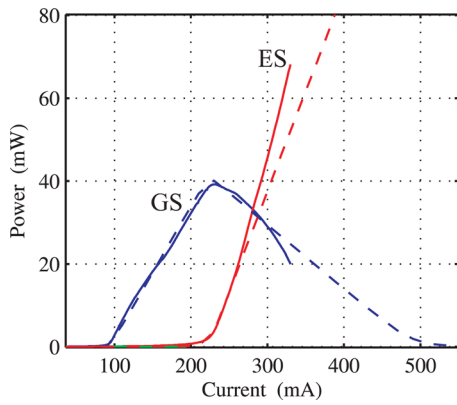


FIG. 10. (Color online) Comparison between measured (solid lines) and simulated (dashed lines) L-I characteristics.

characteristics. The figure shows that our model can reproduce quite well the measured GS roll-off at the ES threshold. Making reference to the input parameters reported in Table I, we used as free parameter the non-radiative life time, the percentage of lasing dots, and the internal quantum efficiency to fit the threshold current and the external quantum efficiency of the GS L-I curve; we used the photon lifetime (and therefore the gain margin) as parameter to fit the separation between GS and ES threshold. The hole transport time was used to fit the slope of the GS roll-off after I_{thES} ; the good fitting of the GS roll-off shown in Fig. 10 was obtained with $\tau_s^h = 50$ ps.

VII. CONCLUSION

This paper shows how the de-synchronization of the electron and hole dynamics in the QD states and the long transport time of the holes in the GaAs barrier can cause the quenching of the GS power when the laser is emitting simultaneously from the GS and ES. The results presented have been obtained with a rate equation model which includes as variables the electrons/holes in the QD confined states, in the WL and also in the SCH and the GS and ES photon density. The model has been used to analyze the two-state lasing L-I characteristic, the carrier occupation in the electron and hole resonant states versus current and the carrier and photon dynamics during the transients due various current steps. The results have shown that, including the holes, the occupation of the lasing GS and ES in conduction and valence band is never clamped at the threshold value, but the electron and hole densities increase and/or decrease with current to maintain the gain clamped. These trends have been used to explain the GS power roll-off and to find the parameters necessary to compare the model results with the available experimental measurements.

ACKNOWLEDGMENTS

The author thanks Professor Levon Asryan (Virginia Polytechnic Institute, Blacksburg, USA) and Professor Ivo Montrosset (Politecnico di Torino, Torino, Italy) for the fruitful discussions and Dr. Mattia Rossetti (Politecnico di Torino, Torino, Italy) for carefully reading the manuscript. Lukas Drzewietzki and Professor Wolfgang Elsässer of Technical University of Darmstadt are also acknowledged for providing the experimental data.

- ¹A. Markus, J. X. Chen, C. Paranthoen, A. Fiore, C. Platz, and O. Gauthier-Lafaye, *Appl. Phys. Lett.* **82**, 121818 (2003).
- ²M. Sugawara, N. Hatori, H. Ebe, M. Ishida, Y. Arakawa, T. Akiyama, K. Otsubo, and Y. Nakata, *J. Appl. Phys.* **97**, 043523 (2005).
- ³C. L. Tan, Y. Wang, H. S. Djie, and B. S. Ooi, *Appl. Phys. Lett.* **91**, 061117 (2007).
- ⁴Z. Y. Zhang, Q. Jiang, and R. A. Hogg, *Electron. Lett.* **46**, 161155 (2010).
- ⁵Q. Cao, S. F. Yoon, C. Z. Tong, C. Y. Ngo, C. Y. Liu, R. Wang, and H. X. Zhao, *Appl. Phys. Lett.* **95**, 191101 (2009).
- ⁶A. Kovsh, I. Krestnikov, D. Livshits, S. Mikhlin, J. Weimert, and A. Zhukov, *Opt. Lett.* **32**, 793 (2007).
- ⁷H. S. Djie, B. S. Ooi, X.-M. Fang, Y. Wu, J. M. Fastenau, W. K. Liu, and M. Hopkinson, *Opt. Lett.* **32**, 44 (2007).
- ⁸L. Chi-Sen, G. Wei, B. Debashish, and B. Pallab, *Appl. Phys. Lett.* **96**(10), 101107 (2010).
- ⁹N. A. Naderi, F. Grillot, K. Yang, J. B. Wright, A. Gin, and L. F. Lester, *Opt. Express* **18**, 27028 (2010).
- ¹⁰A. Markus, J. X. Chen, O. Gauthier-Lafaye, J. G. Provost, C. Paranthoen, and A. Fiore, *IEEE J. Sel. Top. Quantum Electron.* **9**, 1308 (2003).
- ¹¹H. H. Nilsson, J.-Z. Zhang, and I. Galbraith, *Phys. Rev. B* **72**, 205331 (2005).
- ¹²P. Borri, S. Schneider, W. Langbein, and D. Bimberg, *J. Opt. A: Pure Appl. Opt.* **8**, S33 (2006).
- ¹³E. A. Viktorov, P. Mandel, Y. Tanguy, J. Houlihan, and G. Huyet, *Appl. Phys. Lett.* **87**, 053113 (2005).
- ¹⁴H. D. Summers and P. Rees, *J. Appl. Phys.* **101**, 073106 (2007).
- ¹⁵M. Gioannini and M. Rossetti, *IEEE J. Sel. Top. Quantum Electron.* **17**, 51318 (2011).
- ¹⁶L. Asryan, Y. Wu, Yuchang, and R. A. Suris, *Appl. Phys. Lett.* **98**(13), 131108 (2011).
- ¹⁷M. Ishida, Y. Tanaka, K. Takada, T. Yamamoto, S. Hai-Zhi, Y. Nakata, M. Yamaguchi, M. Nishi, M. Sugawara, and Y. Arakawa, *22nd IEEE International Semiconductor Laser Conference (ISLC), 2010*, Kyoto, Japan, 26-30 September, pp. 174–175.
- ¹⁸K. Ludge and E. Scholl, *IEEE J. Quantum Electron.* **45**, 111396 (2009).
- ¹⁹G. Ozgur, A. Demir, and D. G. Deppe, *IEEE J. Quantum Electron.* **45**, 101265 (2009).
- ²⁰L. Coldren and S. Corzine, *Diode Lasers and Photonic Integrated Circuits* (Wiley, New York, USA, 1995), pp. 184–195.
- ²¹C. Z. Tong, S. F. Yoon, C. Y. Ngo, C. Y. Liu, and W. K. Loke, *IEEE J. Quantum Electron.* **42**, 111175 (2006).
- ²²T. R. Nielsen, P. Gartner, and F. Jahnke, *Phys. Rev. B* **69**, 235314 (2004).
- ²³M. Gioannini and I. Montrosset, *IEEE J. Quantum Electron.* **43**, 10941 (2007).
- ²⁴G. A. P. Thè, M. Gioannini, and I. Montrosset, *Opt. Quantum Electron.* **40**, 14-1111-1116 (2008).
- ²⁵D. S. Han and L. V. Asryan, *Nanotechnology* **21**, 015201 (2010).
- ²⁶T. B. Norris, K. Kim, J. Urayama, Z. K. Wu, J. Singh, and P. K. Bhattacharya, *J. Phys. D* **38**, 2077 (2005).
- ²⁷L. C. Su and M. H. Mao, *International Conference on Numerical Simulation of Semiconductor Optoelectronic Devices, NUSOD '06* (Singapore, 2006).